Efficient Single-Photon Sources Based on Chlorine-Doped ZnSe Nanopillars with Growth Controlled Emission Energy

Yurii Kutovyi [a], Marvin Marco Jansen [a], Siqi Qiao [a], Christine Falter [a], Nils von den Driesch [a], Thorsten Brazda [a], Natalia Demarina [b], Stefan Trellenkamp [c], Benjamin Bennemann [d], Detlev Grützmacher [a], and Alexander Pawlis [a*]*

[a] Peter Grünberg Institute (PGI-9), Forschungszentrum Jülich GmbH, 52428 Jülich, Germany and JARA-Fundamentals of Future Information Technology, Jülich-Aachen Research Alliance, 52074 Aachen, Germany

[b] Peter Grünberg Institute (PGI-2), Forschungszentrum Jülich GmbH, 52428 Jülich, Germany

[c] Helmholtz Nano Facility (HNF), Forschungszentrum Jülich GmbH, 52428 Jülich, Germany

[d] Peter Grünberg Institute (PGI-10), Forschungszentrum Jülich GmbH, 52428 Jülich, Germany

*Email: a.pawlis@fz-juelich.de, y.kutovyi@fz-juelich.de

KEYWORDS. Single-photon source, quantum emitter, donor-bound exciton, ZnSe/ZnMgSe quantum well, nanopillar, nanolens, external quantum efficiency.

ABSTRACT. Isolated impurity states in epitaxially grown semiconductor systems possess important radiative features such as distinct wavelength emission with a very short radiative lifetime and low inhomogeneous broadening which makes them promising for the generation of indistinguishable single photons. In this study, we investigate chlorine-doped ZnSe/ZnMgSe quantum well (QW) nanopillar (NP) structures as a highly efficient solid-state single-photon source operating at cryogenic temperatures. We show that single photons are generated due to the radiative recombination of excitons bound to neutral Cl atoms in ZnSe QW and the energy of the emitted photon can be tuned from about 2.85 down to 2.82 eV with ZnSe well width increase from 2.7 to 4.7 nm. Following the developed advanced technology we fabricate NPs with a diameter of about 250 nm using a combination of dry and wet-chemical etching of epitaxially grown ZnSe/ZnMgSe QW well structures. The remaining resist mask serves as a spherical- or cylindrical-shaped solid immersion lens on top of NPs and leads to the emission intensity enhancement by up to an order of magnitude in comparison to the pillars without any lenses. NPs with spherical-shaped lenses show the highest emission intensity values. The clear photon-antibunching effect is confirmed by the measured value of the second-order correlation function at a zero time delay of 0.14. The developed single-photon sources are suitable for integration into scalable photonic circuits.

INTRODUCTION

Quantum emitters producing identical single photons on demand are a key element for the realization of photonic components in quantum information technologies.[1,2] Over the last two decades, significant research efforts have been devoted to develop stable and reliable single-photon sources (SPSs) showing highly efficient and scalable performance. As a result, different kinds of

emitters able to maintain single-photon emission on-demand have been recently demonstrated including sources based on semiconductor quantum dots (QDs),[3–6] single molecules,[7] trapped ions,[8,9] isolated defects[10,11] and impurities,[12–14] or even nonlinear processes such as spontaneous parametric down-conversion.[15] Among the solid-state systems, self-assembled QDs are commonly considered to be superior candidates as high-quality SPSs. These emitters are reported to demonstrate near-ideal state-of-the-art performances generating single photons with high spectral purity and single-photon indistinguishability even at high temperatures.[6,16] Moreover, certain types of QDs have been shown to exhibit the emission of single photons in a wide spectral range from deep ultraviolet to the near-infrared covering even telecommunication bands which makes them particularly attractive for fiber-based quantum networks.[17] However, spectral broadening above the natural linewidth of excitonic states due to charge noise and dephasing perturbations[18] as well as a yet unsolved challenge on the scalability and thus mass-production[19] of self-assembled QDs are the main issues of QD SPSs. These challenges significantly impact the effectiveness of such emitters for practical quantum applications and thus motivate a further search for an ideal SPS with ultimate emission properties.

Recently, single-photon emitters based on isolated impurities hosted in epitaxially grown compound semiconductors have emerged as alternative solid-state emitters demonstrating the ability to generate indistinguishable and high-purity single photons with a short radiative lifetime.[12,20] The emission of single photons in such devices is typically attributed to radiative recombination of excitons bound to spatially isolated shallow impurities (e.g. donors, acceptors).[20] It should be noted that due to the discrete nature of bound exciton energy states in such semiconductor systems, the single photons can be generated through the relevant optical transitions in a well-defined spatial and polarization mode (i.e. in the same quantum state), which in the ideal

case makes each photon naturally indistinguishable from all the others subsequently generated by the same device. Such a feature is a crucial prerequisite of many quantum phenomena for example two-photon interference and therefore is highly required for future applications of photonic quantum emitters.[21]

Zinc Selenide (ZnSe) has been intensively investigated over the last few decades as a promising II-VI semiconductor material with a direct bandgap possessing excellent properties for optical and electronic applications.[22–24] In this regard, ZnSe has emerged as a promising host crystal matrix for impurity-bound-exciton-related emission of single photons.[13,14] In particular, the ability to generate indistinguishable single photons was recently demonstrated with Fluorine (F) donors, spatially isolated in epitaxially grown ZnSe/ZnMgSe QW nanostructures (i.e. ZnSe:F).[12] It should be noted that no tuning was applied to match the emission wavelength of two independent ZnSe:F emitters in that case which reflects a low device-to-device spectral variation for the impurity-based SPSs. However, due to inhomogeneous broadening of the emission wavelength as a result of strong charge fluctuations, the indistinguishability of only 65% has been measured for ZnSe:F sources. Despite that, the successful generation of substantial polarization entanglement between photons generated by independent F-impurity-based emitters was also reported[13] and comprises an essential step towards the realization of long-distance quantum communication and networking. Furthermore, recent publications also showed that ZnSe:F provides isolated impurity-bound electrons which can be effectively used as optically addressable spin qubits.[14] Such features of ZnSe:F make it particularly attractive for modern quantum applications and therefore motivate further research of other impurities in epitaxially grown ZnSe.

More recently, Chlorine (Cl) impurities in ZnSe (i.e. ZnSe:Cl) were suggested as alternative impurity-based SPSs demonstrating stable and bright emission of single photons.[25] Similar to the

F-impurity, Cl substitutes the Se atom in the ZnSe crystal yielding a shallow donor impurity. However, in contrast to F, Cl has an atomic radius that is comparable with that of the Se atom making Cl a perfect donor on the Se site that considerably better matches into the ZnSe crystal and therefore does not naturally form other impurity states in ZnSe. As a result, a much higher degree of indistinguishability can be expected for ZnSe:Cl emitters compared to ZnSe:F. Although the latter expectation has to be proven yet, Cl impurities in ZnSe indeed consolidate the advantages of F-donors to be exploited as reliable single-photon emitters as shown in the recent investigation performed by Karasahin et al.[25] In particular, the reported time-resolved photoluminescence measurements[25] revealed radiative lifetimes of single photons emitted by Cl donors in ZnSe QWs as short as 192 ps and an emission frequency jitter of less than 14 GHz, both aspects demonstrating the certain potential of realizing a so-called "lifetime-limited" SPSs. However, it should be noted that the related study[25] has been performed exclusively for unstructured Cl-doped ZnSe/ZnMgSe QW samples and didn't attempt to produce an independent device that can be integrated into a photonic quantum circuit.

In this work, we are going beyond existing research by presenting an advanced nanofabrication concept and report on the optical performance of independent Cl-bound quantum emitters developed and fabricated in form of ZnSe/ZnMgSe QW NP structures which are directly integrated with three-dimensional all-dielectric solid immersion lenses (SILs) to improve the external quantum efficiency of the devices. The employment of SILs for such purposes has been extensively discussed and shown in the literature over the last few decades for a variety of emitters.[26,27] It has been revealed that SILs are a suitable remedy to overcome the total internal reflection problem[26] which is the origin of the low collection efficiency of the emitted radiation coming out from the emissive material. For instance, the use of a SIL with a refractive index

smaller than the refractive index of the semiconductor usually results in increased external quantum efficiency. With this in mind, we advanced a nanopillar fabrication technology approach[12] allowing us firstly to fabricate a SIL and then directly use it as a hard mask for the subsequent etching of the NP. It should be noted that in this case, fabricated nanolenses don't require any post-fabrication alignment and positioning as they become directly coupled with the NP emitters after the etching. We demonstrate that the developed approach allows for the fabrication of highly efficient quantum emitters with enhanced external quantum efficiency and high emission rates of antibunched photons. In addition, we address a common problem of spectral variability between photons generated by different devices. In this regard, we numerically and experimentally demonstrate that our engineered devices can effectively generate single photons with pre-defined emission energies which reveals the substantial potential of our ZnSe:Cl SPSs to form reliable optical quantum links in future quantum networks.

RESULTS AND DISCUSSION

Device concept and single-photon emission properties. Figure 1a shows a schematic illustration of the developed single-photon emitter which consists of a ZnSe/ZnMgSe QW NP structure coupled with spherical-shaped HSQ nanolens. The operation principle of the device is based on the radiative recombination of excitons which are bound to a single spatially isolated Cl donor in an epitaxially grown ZnSe/ZnMgSe QW (see Section 1 in the Supporting information). A typical photoluminescence (PL) spectrum measured for an NP structure at a temperature of 5 K is shown in Figure 1b. The sharp line which we attribute to the emission of single photons due to the radiative decay of the Cl-bound exciton complex has been observed at about 2.848 eV. The origin of the peak is confirmed by the PL intensity of the line measured as a function of the excitation

power for the NP device with a spherical-shaped HSQ lens at a temperature of 7 K (see Figure 2a). As can be seen in Figure 2a, the intensity of the narrow D^0X peak exhibits a superlinear power-function dependence ($I \propto P^{1.13\pm0.05}$) in the low excitation regime (i.e. $P \leq 10$ µW). The observed superlinear increase of the D^0X intensity with the excitation power might originate from the reduced volume of QW NP structures, which upon excitation yields a higher carrier concentration in the energy bands compared to the bulk material and thus results in an increased recombination probability of the donor-bound excitons at low excitation powers. In contrast, for unstructured ZnSe:Cl QW samples a nearly linear emission dependence on the excitation power for bound- and free-excitons was reported[25] with $P^{0.98}$ and $P^{1.06}$, respectively. The dependence starts to saturate with a further increase of the excitation power which is typical for the impurity bound-exciton emission.[25] At the same time, a group of peaks associated with the emission from heavy-hole free-excitons is observed in the energy region higher than 2.860 eV. It should be noted that the presence of several peaks in the FX group can be attributed to monolayer fluctuations of the QW width in the sample resulting in digital variations of the excitonic transitions. As can be seen in Figure 1b, the energy separation between D^0X and FX emission is about 12 meV in this specific case, which provides substantial spectral independence and stability. Such a large separation results from the enhanced binding energy of the donor-bound excitons in the two-dimensional QW[25] and potentially enables operation even at elevated temperatures (<80 K). However, it should be noted that thermal energy remains the limiting factor for donor-bound-exciton-based emitters. Once it reaches the same order as the ionization energy of the donor-bound-exciton transition (e.g. 12-15 meV), a substantial reduction of the radiative quantum efficiency of the SPS is expected due to the non-radiative dissociation of shallow-donor bound-exciton complexes.

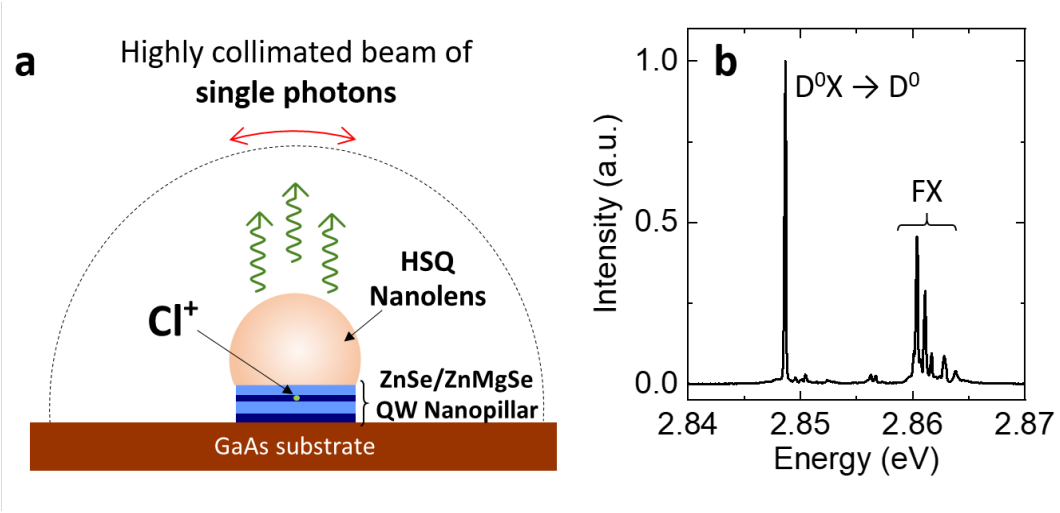

Figure 1. (a) Schematic illustration of a Cl-doped ZnSe/ZnMgSe QW NP with spherical-shaped HSQ nanolens on top that helps to collect the emitted photons. (b) Typical PL spectrum measured for a ZnSe/ZnMgSe NP (ZnSe QW width of approximately 2.71 nm) with a spherical-shaped lens at a temperature of 5 K and with 5 μW pulsed laser excitation. The spectrum reveals a single-photon emission line at 2.848 eV that originates from the recombination of donor-bound excitons ($D^0X \rightarrow D^0$). The FX-labeled group of peaks corresponds to the recombination of heavy-hole free excitons.

To reveal that the fabricated Cl-doped ZnSe/ZnMgSe QW NPs are high-quality quantum emitters capable to emit single photons with high flux, we performed power-dependent PL measurements as well as time-correlated single-photon counting measurements.

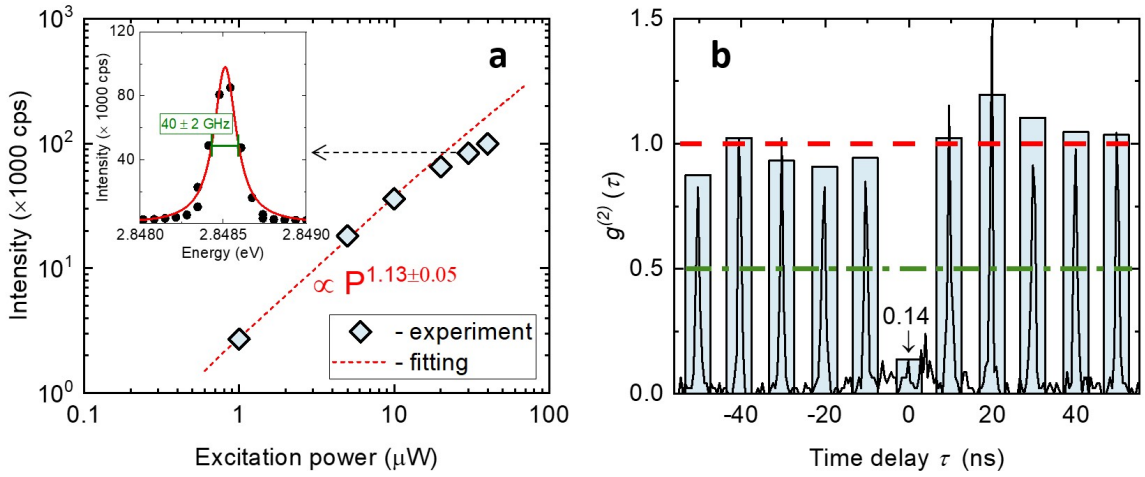

Figure 2. (a) Intensity of the D^0X line (spectral shape shown in the inset) as a function of the excitation power measured at a temperature of 7 K. Dashed red line represents a linear fitting of the experimental data (in the log-log scale) measured at low-power excitations (≤ 10 μW). Inset: D^0X peak of the PL spectrum measured at 30 μW as pointed out by the dashed arrow. (b) Normalized photon correlation histogram that was measured for the same NP device with the power dependence and the linewidth presented in Figure 2a. For the $g^{(2)}$-measurement, an excitation power of 30 μW was chosen.

Figure 2b displays the normalized photon-correlation histogram measured for the donor-bound exciton emission from a typical NP emitter. The corresponding D^0X emission line is shown in the inset of Figure 2a and was fitted with the Lorentz function yielding the spectral full-width-at-half-maximum (FWHM) of (40±2) GHz. It should be noted the FWHM of 40 GHz is limited by the resolving power of our spectrometer (see Methods) and is expected to be significantly smaller in the fabricated devices. At the same time, due to the high emission rate of the NP under investigation, an integration time of only 30 min was sufficient to achieve a clear coincidence correlation histogram. As can be seen in Figure 2b, the height of the central coincidence peak at

zero delay time is considerably reduced revealing the clear photon-antibunching effect. In this exemplary case, we observed residual two-photon probability of $g^{(2)}(0)$ to be 0.14 ± 0.02 calculated from the ratio of the height of the central coincidence peak to the 20 averaged adjacent peaks ($\tau \neq 0$) and without any background subtraction. It should be noted that the obtained value of $g^{(2)}(0) = 0.14 \pm 0.02$ is well below the threshold value of 0.5 for quantum emitters.[12,25] We thus observe a clear single-photon antibunching emission from the single chlorine donor even at relatively high excitation powers (i.e. at 30 μW).

Spectral tuning of quantum emission. Spectral tuning is an essential aspect of the practical applications of single-photon sources in photon-based information processing schemes and readout protocols.[12,28] Note that the ability to fine-tune the PL emission and thus entangle single photons emitted from independent F-donors in ZnSe QW nanostructures has been recently shown using a local laser heating method.[13] The temperature fine-tuning of the emission wavelength for the developed ZnSe:Cl NP emitters is presented and discussed in the Supporting information (see Section 3). Below, we combine simulation and experiments to demonstrate the spectral coarse-tuning possibility for the developed single-photon emitters by engineering the ZnSe QWs with different widths.

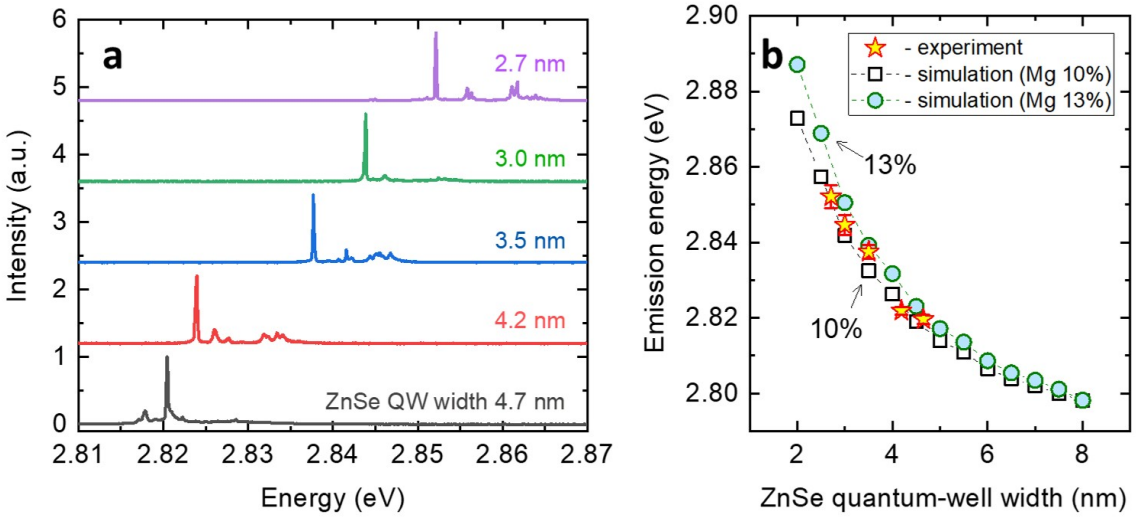

Figure 3. Coarse-tuning of single-photon emission. (a) Typical PL spectra measured for the NPs with different ZnSe QW widths under the same experimental conditions. The shift of the D^0X emission peak reflects the wavelength coarse-tuning of our developed NPs. (b) PL emission energy of the donor-bound-exciton as a function of ZnSe QW width obtained for experimental and simulated data. The simulations were performed for ZnMgSe/ZnSe/ZnMgSe QW stacks with 10 % and 13 % Mg concentration, respectively, as typical Mg contents in the ZnMgSe barriers of the measured samples. Vertical error bars in the experimental data represent the standard deviation of the mean values calculated for each set of studied NPs with different QW widths.

Figure 3a displays typical PL emission spectra measured for chlorine-delta-doped NPs with different ZnSe QW widths. In this specific case, the PL measurements were performed at a temperature of 10 K and 5 µW excitation power using the NPs exhibiting a clear D^0X emission related to the Cl-donor. As can be seen in Figure 3a, the emission energy of the bound-exciton PL shifts towards higher energy with decreasing QW width and allows for coarse-tuning of the emission wavelength. Figure 3b depicts the measured D^0X peaks as a function of the ZnSe QW width. A pronounced redshift of the emission energy with increasing the QW width is observed.

We attribute this redshift to the change of the QW confinement, also altering the exciton binding energy as a function of the QW width.[29] Moreover, as can be seen in Figure 3b, shrinking the QW width from 4.7 to 2.7 nm increases the emission energy of the D^0X peak by 30 meV. This wide tuning range reveals the enormous effect of QW confinement on bound-exciton-related emission allowing us to precisely engineer and fabricate single-photon emitters with practically pre-defined emission properties. In particular, coarse-tuning of the emission wavelength to roughly 436 nm is required for interfacing to trapped Yb^+ ions, for example, via direct coupling to its 435.5 nm clock transition[30] or using frequency conversion with a hydrogen pressure cell to interface the 369.5 nm transition of Yb^+ ions.[31] Both might allow for employing schemes of quantum networking between our developed SPSs and trapped ions as quantum memories.

To confirm our interpretation of the PL tuning experiments presented in Figure 3b, we calculated the D^0X binding energy in ZnSe/ZnMgSe QW structures with a theoretical model (see Methods) involving a nonvariational approach to density-functional theory[32,33] closely following the routine presented in Ref[33]. The calculated dependencies of the D^0X emission energy as a function of ZnSe QW width are shown in Figure 3b. The calculations were performed for the ZnSe/ZnMgSe QW samples with 10 % and 13 % Mg concentration, respectively, as typical frame-values for the studied devices. As can be seen in Figure 3b, the obtained calculation results show an excellent agreement with the experimental data.

Finally, we present a specifically developed fabrication concept for Cl-doped ZnSe/ZnMgSe NPs which are directly integrated with HSQ-based SILs (see Methods). Below we demonstrate and discuss the effect of SILs on top of the developed SPS comparing the optical performance of the NPs with spherical- and cylindrical-shaped HSQ nanolenses as well as without any lens. The latter pillars were obtained after chemical etching with 1%-HF of the corresponding RIE-etched

samples. Note that spherical-shaped lenses were intentionally defined by the performed grayscale electron-beam lithography and can be later further shaped using different etch chemistries (see Methods as well as Section 2 in the Supporting information for more details). Figures 4(a) and 4(b) displays the histogram plots of the D^0X peak intensities measured for a set of pillars with and without HSQ lenses and processed with H_2/Ar and H_2/Ar/CHF_3 RIE plasmas, respectively. In this case, PL measurements for all pillars were performed under the same experimental conditions at a temperature of 5 K and 5 μW excitation power.

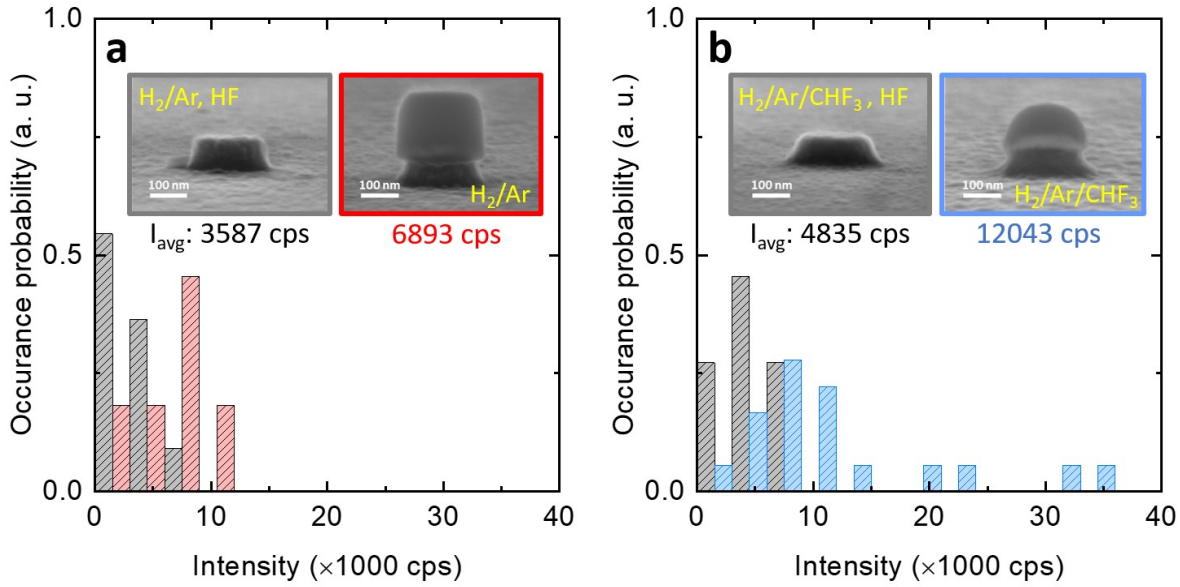

Figure 4. The histograms of the PL intensity distributions measured for the D^0X emission from NPs with and without HSQ lenses etched using (a) H_2/Ar or (b) H_2/Ar/CHF_3 RIE plasma. The histogram bin-width of 3000 cps is used. The mean average values of each intensity distribution are indicated under the corresponding SEM insets which represent a typical NP for each set of measured devices. For the NPs covered with spherical-shaped HSQ nanolenses and etched using H_2/Ar/CHF_3 RIE plasma (shown in blue), we observe up to one order of magnitude increase in the external quantum efficiency.

As can be seen in Figures 4(a) and 4(b), the measured intensity of the D^0X emission for all studied emitters is statistically distributed with the mean values indicated in the plots. Intensity variations of about an order of magnitude are observed for all kinds of investigated devices regardless of the type and presence of the lens. Such behavior reflects a typical inhomogeneity issue for solid-state emitters[10,13] and can be attributed to lateral variations of donor position for different studied pillars. Our theoretical estimations using a geometrical ray-tracing approach presented in the Supporting information (see Section 4) reveal at least a factor of four for the intensity change between donor position in the center compared to that at the edge of the NPs covered with the spherical-shaped lenses. At the same time, for the devices with cylindrical-shaped lenses, a factor of about two was obtained. In this regard, on-demand single-dopant implantation technology[34] allowing for more precise positioning of individual donors in the NP would be the possible solution to reduce a device-to-device intensity variation related to the position of the optically active single donor (i.e. point-like source).

Despite the observed device inhomogeneity issue, a substantial improvement in the PL intensity for the pillars covered with cylindrical- and spherical-shaped HSQ lenses is well-pronounced and can be clearly evidenced in Figures 4(a) and 4(b), respectively. In particular, we see that the ratios between the average count rates for H_2/Ar and H_2/Ar/CHF_3-etched pillars without and with lenses are about 1:1.75 and 1:2.49, respectively. Additionally, we see that the ratio between the average count rates for H_2/Ar and H_2/Ar/CHF_3-etched pillars is about 1:1.35 when the lenses are removed with 1%-HF. This indicates a substantial positive impact of CHF_3 gas at low flow rates in the H_2/Ar/CHF_3 plasma on the internal quantum efficiency in the pillars due to the less-damaged side-wall surfaces compared to those obtained after dry etching with H_2/Ar only.

Moreover, the effect of using HSQ as a mask and solid immersion lens is at least twofold: Firstly, by using HSQ material (i.e. glass-like SiO_2) with a low refractive index on top of the ZnSe/ZnMgSe NPs, we reduced the gradient in the refractive index change between semiconductor and environment, which leads to an increased total internal reflection angle and with that, better outcoupling efficiency.[26] This effect is also confirmed by numerical simulations performed using Lumerical simulation software. The simulation results are presented in the Supplementary information (see Section 5) and reveal that the presence of HSQ on top of ZnSe/ZnMgSe QW NPs offers up to 135% PL intensity enhancement, which is consistent with our experimental findings. This demonstrates substantial improvement in the outcoupling efficiency for NPs covered with HSQ.

Secondly, at the same time, NPs with spherical-shaped HSQ lenses generally demonstrate higher count rates compared to the devices covered with cylindrical-shaped HSQ. This partially reflects the effect of the spherical-shaped HSQ lens working as a plano-convex lens and effectively collimating the generated single photons into a smaller numerical aperture (see Figure S6c in the Supporting information). To emphasize the importance of the spherical-shaped SILs on top of the ZnSe:Cl NPs, we also estimated the photon extraction efficiency (PPE) for our SPSs following the PPE determination procedure reported in Ref.[27] Assuming the geometrical averaged setup efficiency of about 4% and considering NPs showing the highest brightness (see Figure 4(b)), we deduced the PPE of about 0.9% for sources excited non-resonantly with our pulsed laser ($f = 100\,MHz$) at 5 µW excitation power. At the same time, considering the excitation-power-dependent emission of the D^0X line reported in Figure 2(a), we determine the PEE as high as 6.3% at the saturation power of 35 µW." However, although the results above demonstrate that spherical-shaped HSQ lenses offer the highest external quantum efficiency among the investigated

devices, the latter could still be further improved. In particular, our simulations performed with Lumerical software (see Section 6 in the Supporting information) show that the inclusion of an about 180 nm thick HSQ spacer below the spherical HSQ lens allows achieving an additional increase in the quantum efficiency due to the Purcell effect enhancement that is maximized at this condition. Moreover, further optimizations, which would lead to an even higher quantum efficiency of the developed sources are still possible. For instance, an AlAs layer can be introduced below ZnSe/ZnMgSe QW which can be later wet-oxidized into an Al_2O_3 layer allowing to decouple ZnSe/ZnMgSe QW NP from the absorbing GaAs substrate. In this case, Al_2O_3 also forms an etch stop layer allowing to perform selective removal of the GaAs below the NP structures, and subsequently, deposit metal coatings (e.g. deposition of Al, Cr, or Ag) on the backside surface to produce a metal mirror specifically below the NP emitters. With such a metallic mirror coating below the NPs, the quantum efficiency of our ZnSe:Cl emitters is expected to increase by nearly a factor of two.

CONCLUSION

Optically active impurities in epitaxially grown II-VI semiconductors offer a great opportunity to produce identical single photons on demand. In this study, we reported highly efficient single-photon emission as a result of the radiative recombination of excitons bound to single Cl donors which were intentionally isolated in ZnSe/ZnMgSe QW NPs. By photon auto-correlation measurements, we verified single-photon antibunching for the devices hosting a single Cl-donor. A distinct spectral coarse-tuning up to 30 meV was experimentally and numerically demonstrated by engineering QWs with different widths. To improve the collection efficiency of single photons, we developed and fabricated NPs that are directly integrated with solid immersion nanolenses

made of HSQ. As a result, a significant enhancement of the average external quantum efficiency by a factor of 2.5 for the devices with spherical-shaped HSQ nanolenses was achieved. These results provide a promising advance towards ZnSe:Cl-based single-photon sources as highly efficient and spectrally tunable devices to be applied in quantum computing and optically mediated quantum information processing technology.

METHODS

Sample fabrication. The ZnSe/ZnMgSe QW nanopillars were fabricated on top of commercially available GaAs substrates with (100) crystallographic orientation. The details of the fabrication process flow can be found in the Supporting information (see Section 2). Briefly, epitaxial growth of Cl-doped ZnSe/ZnMgSe QWs was performed on GaAs substrates using molecular beam epitaxy (MBE). After MBE growth, the nanostructuring based on a top-down fabrication approach was carried out to pattern NP structures with SILs on top and thus isolate individual Cl impurities in ZnSe QWs. First, grayscale electron-beam lithography was employed to define nanolenses with a given size and shape in the HSQ resist. Next, the reactive ion etching (RIE) was performed to etch ZnSe/ZnMgSe NPs. Two recipes were developed and used for this purpose: In the first recipe, the ZnSe/ZnMgSe QW multilayer stack was etched using a gas mixture of hydrogen (H_2) and argon (Ar) leading to a cylindrical shape of the HSQ lenses. The second dry etching recipe is based on the mixture of H_2, Ar, and CHF_3 gases and was effectively used to pattern NPs with spherical-shaped HSQ nanolenses on top. The wet-chemical polishing using a water-based solution of potassium dichromate ($HBr:K_2Cr_2O_7:H_2O$) was then performed to remove any near-surface defects in the NPs introduced during the RIE step. Finally, to prevent oxidation and thus

degradation of the nanostructures, all the samples were immediately passivated with 10 nm Al_2O_3 oxide deposited using an atomic layer deposition system.

Optical characterization. The nanostructures were excited non-resonantly at a wavelength of 394 nm using a pulsed frequency-doubled Ti:Sapphire laser with a pulse width of 80 fs working at a repetition frequency of 100 MHz. First, the emitted PL was collected using a high numerical aperture objective lens (NA = 0.9). Then, the emission was directed through a 1000 μm pinhole, dispersed with a 2400 lines holographic grating, and gathered to the CCD camera of a Princeton Instruments Acton SP 2500 monochromator with a 500 mm focal length. This system yields a spectral resolution of about 40 GHz at a 20 μm slit opening. For the two-photon correlation, the emission was filtered by the same monochromator system and transferred to a Hanbury-Brown-Twiss setup employing a 50/50 beam splitter and two single-photon sensitive avalanche photodiodes (Micro Photon Devices, PicoQuant) with timing resolution down to 50 ps. A time-correlated single-photon counting module (PicoHarp 300, PicoQuant) providing a channel resolution of 4 ps was used to perform the antibunching experiments.

Calculation of the D^0X binding energy in ZnSe/ZnMgSe QW structure. The calculation of the D^0X binding energy in ZnSe/ZnMgSe QW was performed considering the D^0X complex consisting of a neutral donor, two electrons, and a hole (see Figure S1 in the Supporting information). The electron or hole effective Hamiltonian in the Kohn-Sham basis includes terms describing Coulomb interaction between the particles, the particles and the impurity ion as well as exchange-correlation interaction. During the sample growth, the ZnSe QWs are delta-doped in the middle thus in the calculations the Cl donors are assumed to be located at the center of the ZnSe QW. The form of the interaction-correlation potential is chosen following Refs[33,35]. The effective Hamiltonian for an electron and a hole can be decomposed into two parts: The first part represents

the QW confinement while the second describes the motion in the plane perpendicular to the direction of the layer growth. The valence and conduction band discontinuities for ZnSe/ZnMgSe QWs are calculated taking into account the assumption that ZnSe and ZnMgSe layers are compressively strained being pseudomorphically grown on the GaAs substrate.[36] The electronic and structural parameters of ZnSe and ZnMgSe used for the calculations are taken from Refs[37,38]. Material parameters for $Zn_{1-x}Mg_xSe$ are obtained assuming that they change linearly with the Mg concentration. The calculated position of the conduction and valence bands and the component of the wave functions in the direction perpendicular to the layer growth for the Cl-doped ZnSe QW are shown in Figure S13 in the Supporting information. The slight bending of the bands is due to the electrical field associated with the ionized Cl atoms. To calculate the D^0X binding energy, the ground-state energy of the neutral impurity as well as the ground-state energy of the free exciton[39] should be subtracted from the total energy of the system obtained as a result of solving the Kohn-Sham equation. Then the transition energy is calculated by subtracting the free exciton and D^0X binding energies from the ZnSe band gap determined by the calculated electron and heavy hole ground-state energies.

ASSOCIATED CONTENT

Supporting Information

The Supporting Information is available free of charge at https://pubs.acs.org/doi/XXXXX.

It contains supplementary figures and details on the working principle of the Chlorine-donor-based single-photon emitter; a detailed description of the device fabrication technology; supplementary simulation and calculation results on external quantum efficiency; supplementary band diagram of

ZnMgSe/ZnSe/ZnMgSe QW nanostructure and fine-tuning of the spectral emission by sample temperature.

AUTHOR INFORMATION

Corresponding Author

*Email: a.pawlis@fz-juelich.de, y.kutovyi@fz-juelich.de

Author Contributions

The manuscript was written with the contributions of all authors. All authors have approved the final version of the manuscript.

Funding Sources

This work is supported by Deutsche Forschungsgemeinschaft (DFG, German Research Foundation) under Germany's Excellence Strategy Cluster of Excellence: Matter and Light for Quantum Computing (ML4Q) (EXC 2004 1-390534769).

Notes

The authors declare no competing financial interest.

ACKNOWLEDGMENT

The authors acknowledge support from the technical staff of the Helmholtz Nano Facility (HNF) of Forschungszentrum Jülich for their assistance with the fabrication of the single-photon emitters. The authors thank Aziz Karasahin (the University of Maryland) for the help with the time-correlated single-photon counting measurements and discussion of antibunching experiments. This work is supported by Deutsche Forschungsgemeinschaft (DFG, German Research Foundation)

under Germany's Excellence Strategy Cluster of Excellence: Matter and Light for Quantum Computing (ML4Q) (EXC 2004 1-390534769).

ABBREVIATIONS

QW, quantum well; NP, nanopillar; HSQ, hydrogen silsesquioxane; SPS, single-photon source; F, fluorine; Cl, chlorine; PL, photoluminescence; MBE, molecular beam epitaxy; SIL, solid immersion lens; RIE, reactive ion etching; HF, hydrofluoric acid; FWHM, full-width-at-half-maximum.

REFERENCES

(1) Senellart, P.; Solomon, G.; White, A. High-Performance Semiconductor Quantum-Dot Single-Photon Sources. *Nat Nanotechnol* **2017**, *12*, 1026–1039. https://doi.org/10.1038/nnano.2017.218.

(2) Slussarenko, S.; Pryde, G. J. Photonic Quantum Information Processing: A Concise Review. *Appl Phys Rev* **2019**, *6*, 041303. https://doi.org/10.1063/1.5115814.

(3) Moczała-Dusanowska, M.; Dusanowski, Ł.; Gerhardt, S.; He, Y. M.; Reindl, M.; Rastelli, A.; Trotta, R.; Gregersen, N.; Höfling, S.; Schneider, C. Strain-Tunable Single-Photon Source Based on a Quantum Dot-Micropillar System. *ACS Photonics* **2019**, *6* (8), 2025–2031. https://doi.org/10.1021/acsphotonics.9b00481.

(4) Srocka, N.; Mrowiński, P.; Große, J.; Schmidt, M.; Rodt, S.; Reitzenstein, S. Deterministically Fabricated Strain-Tunable Quantum Dot Single-Photon Sources Emitting in the Telecom O-Band. *Appl Phys Lett* **2020**, *117* (22), 224001. https://doi.org/10.1063/5.0030991.

(5) Mantynen, H.; Anttu, N.; Sun, Z.; Lipsanen, H. Single-Photon Sources with Quantum Dots in III-V Nanowires. *Nanophotonics* **2019**, *8* (5), 747–769. https://doi.org/10.1515/nanoph-2019-0007.

(6) Paesani, S.; Borghi, M.; Signorini, S.; Maïnos, A.; Pavesi, L.; Laing, A. Near-Ideal Spontaneous Photon Sources in Silicon Quantum Photonics. *Nat Commun* **2020**, *11* (1). https://doi.org/10.1038/s41467-020-16187-8.

(7) Rezai, M.; Wrachtrup, J.; Gerhardt, I. Polarization-Entangled Photon Pairs from a Single Molecule. *Optica* **2019**, *6* (1), 34–40. https://doi.org/10.1364/optica.6.000034.

(8) Kurz, C.; Huwer, J.; Schug, M.; Müller, P.; Eschner, J. A High-Rate Source for Single Photons in a Pure Quantum State. *New J Phys* **2013**, *15*, 055005. https://doi.org/doi:10.1088/1367-2630/15/5/055005.

(9) Higginbottom, D. B.; Slodička, L.; Araneda, G.; Lachman, L.; Filip, R.; Hennrich, M.; Blatt, R. Pure Single Photons from a Trapped Atom Source. *New J Phys* **2016**, *18*, 093038. https://doi.org/10.1088/1367-2630/18/9/093038.

(10) Grosso, G.; Moon, H.; Lienhard, B.; Ali, S.; Efetov, D. K.; Furchi, M. M.; Jarillo-Herrero, P.; Ford, M. J.; Aharonovich, I.; Englund, D. Tunable and High-Purity Room Temperature Single-Photon Emission from Atomic Defects in Hexagonal Boron Nitride. *Nat Commun* **2017**, *8* (1), 1–8. https://doi.org/10.1038/s41467-017-00810-2.

(11) Bogdanov, S. I.; Shalaginov, M. Y.; Lagutchev, A. S.; Chiang, C. C.; Shah, D.; Baburin, A. S.; Ryzhikov, I. A.; Rodionov, I. A.; Kildishev, A. v.; Boltasseva, A.; Shalaev, V. M. Ultrabright Room-Temperature Sub-Nanosecond Emission from Single Nitrogen-Vacancy Centers Coupled to Nanopatch Antennas. *Nano Lett* **2018**, *18* (8), 4837–4844. https://doi.org/10.1021/acs.nanolett.8b01415.

(12) Sanaka, K.; Pawlis, A.; Ladd, T. D.; Lischka, K.; Yamamoto, Y. Indistinguishable Photons from Independent Semiconductor Nanostructures. *Phys Rev Lett* **2009**, *103*, 053601. https://doi.org/10.1103/PhysRevLett.103.053601.

(13) Sanaka, K.; Pawlis, A.; Ladd, T. D.; Sleiter, D. J.; Lischka, K.; Yamamoto, Y. Entangling Single Photons from Independently Tuned Semiconductor Nanoemitters. *Nano Lett* **2012**, *12*, 4611–4616. https://doi.org/10.1021/nl301911t.

(14) Sleiter, D. J.; Sanaka, K.; Kim, Y. M.; Lischka, K.; Pawlis, A.; Yamamoto, Y. Optical Pumping of a Single Electron Spin Bound to a Fluorine Donor in a ZnSe Nanostructure. *Nano Lett* **2013**, *13*, 116–120. https://doi.org/10.1021/nl303663n.

(15) Guo, X.; Zou, C. L.; Schuck, C.; Jung, H.; Cheng, R.; Tang, H. X. Parametric Down-Conversion Photon-Pair Source on a Nanophotonic Chip. *Light Sci Appl* **2017**, *6*, 1–8. https://doi.org/10.1038/lsa.2016.249.

(16) Arakawa, Y.; Holmes, M. J. Progress in Quantum-Dot Single Photon Sources for Quantum Information Technologies: A Broad Spectrum Overview. *Appl Phys Rev* **2020**, *7* (2). https://doi.org/10.1063/5.0010193.

(17) da Lio, B.; Faurby, C.; Zhou, X.; Chan, M. L.; Uppu, R.; Thyrrestrup, H.; Scholz, S.; Wieck, A. D.; Ludwig, A.; Lodahl, P.; Midolo, L. A Pure and Indistinguishable Single-Photon Source at Telecommunication Wavelength. *Advanced Quantum Technologies* **2022**, *5*, 2200006. https://doi.org/https://doi.org/10.1002/qute.202200006.

(18) Stachurski, J.; Tamariz, S.; Callsen, G.; Butté, R.; Grandjean, N. Single Photon Emission and Recombination Dynamics in Self-Assembled GaN/AlN Quantum

Dots. *Light: Science and Applications*. Springer Nature December 1, 2022. https://doi.org/10.1038/s41377-022-00799-4.

(19) Castelletto, S. Silicon Carbide Single-Photon Sources: Challenges and Prospects. *Materials for Quantum Technology* **2021**, *1*, 023001. https://doi.org/10.1088/2633-4356/abe04a.

(20) Pawlis, A.; Sanaka, K.; Götzinger, S.; Yamamoto, Y.; Lischka, K. Investigation of Excitons Bound to Fluorine Donors in ZnSe. *Semicond Sci Technol* **2006**, *21*, 1412–1415. https://doi.org/10.1088/0268-1242/21/10/007.

(21) Lal, N.; Mishra, S.; Singh, R. P. Indistinguishable Photons. *AVS Quantum Science* **2022**, *4*, 021701. https://doi.org/10.1116/5.0083968.

(22) Pawlis, A.; Mussler, G.; Krause, C.; Bennemann, B.; Breuer, U.; Grutzmacher, D. MBE Growth and Optical Properties of Isotopically Purified ZnSe Heterostructures. *ACS Appl Electron Mater* **2019**, *1*, 44–50. https://doi.org/10.1021/acsaelm.8b00006.

(23) Janßen, J.; Hartz, F.; Huckemann, T.; Kamphausen, C.; Neul, M.; Schreiber, L. R.; Pawlis, A. Low-Temperature Ohmic Contacts to n-ZnSe for All-Electrical Quantum Devices. *ACS Appl Electron Mater* **2020**, *2*, 898–905. https://doi.org/10.1021/acsaelm.9b00824.

(24) Gutowski, J.; Presser, N.; Kudlek, G. Optical Properties of ZnSe Epilayers and Films. *Phys. stat. sol. (a)* **1990**, *120* (11), 11–59. https://doi.org/10.1002/pssa.2211200102.

(25) Karasahin, A.; Pettit, R. M.; von den Driesch, N.; Jansen, M. M.; Pawlis, A.; Waks, E. Single Quantum Emitters with Spin Ground States Based on Cl Bound Excitons in ZnSe. *arXiv.org, e-Print Arch., Quantum Phys.* **2022**. https://doi.org/10.48550/arXiv.2203.05748.

(26) Barnes, W. L.; Björk, G.; Gérard, J. M.; Jonsson, P.; Wasey, J. A. E.; Worthing, P. T.; Zwiller, V. Solid-State Single Photon Sources: Light Collection Strategies. *The European Physical Journal D* **2002**, *18*, 197–210. https://doi.org/10.1140/epjd/e20020024.

(27) Gschrey, M.; Thoma, A.; Schnauber, P.; Seifried, M.; Schmidt, R.; Wohlfeil, B.; Krüger, L.; Schulze, J. H.; Heindel, T.; Burger, S.; Schmidt, F.; Strittmatter, A.; Rodt, S.; Reitzenstein, S. Highly Indistinguishable Photons from Deterministic Quantum-Dot Microlenses Utilizing Three-Dimensional in Situ Electron-Beam Lithography. *Nat Commun* **2015**, *6*, 1–8. https://doi.org/10.1038/ncomms8662.

(28) Steiner, M.; Meyer, H. M.; Deutsch, C.; Reichel, J.; Köhl, M. Single Ion Coupled to an Optical Fiber Cavity. *Phys Rev Lett* **2013**, *110* (4), 043003. https://doi.org/10.1103/PhysRevLett.110.043003.

(29) Rueangnetr, N.; Sivalertporn, K. Effect of Quantum Well Width on the Electron and Hole States in Different Single Quantum Well Structures. *J Phys Conf Ser* **2019**, *1380* (1), 1–4. https://doi.org/10.1088/1742-6596/1380/1/012082.

(30) Stenger, J.; Tamm, C.; Haverkamp, N.; Weyers, S.; Telle, H. R. Absolute Frequency Measurement of the 435.5-Nm 171 Yb+-Clock Transition with a Kerr-Lens Mode-Locked Femtosecond Laser. *Opt Lett* **2001**, *26* (20), 1589. https://doi.org/doi.org/10.1364/OL.26.001589.

(31) Olmschenk, S.; Younge, K. C.; Moehring, D. L.; Matsukevich, D. N.; Maunz, P.; Monroe, C. Manipulation and Detection of a Trapped Yb+ Hyperfine Qubit. *Phys Rev A* **2007**, *76* (5). https://doi.org/10.1103/PhysRevA.76.052314.

(32) Kohn, W.; Sham, L. J. Self-Consistent Equations Including Exchange and Correlation Effects*. *Physical Review* **1965**, *140* (4A), A1133–A1138. https://doi.org/10.1103/PhysRev.140.A1133.

(33) Dunn, J. L.; Bates, C. A.; Pye, M. J.; Boffety, D.; Vasson, A.-M.; Vasson, † A; Leymarie, J. Binding Energy of Bound Excitons D0X in Quantum Wells. *Phys Rev B* **1998**, *58* (12), 7970–7977. https://doi.org/10.1103/PhysRevB.58.7970.

(34) Jakob, A. M.; Robson, S. G.; Schmitt, V.; Mourik, V.; Posselt, M.; Spemann, D.; Johnson, B. C.; Firgau, H. R.; Mayes, E.; McCallum, J. C.; Morello, A.; Jamieson, D. N. Deterministic Shallow Dopant Implantation in Silicon with Detection Confidence Upper-Bound to 99.85% by Ion–Solid Interactions. *Advanced Materials* **2022**, *34*, 2103235. https://doi.org/10.1002/adma.202103235.

(35) Wunsche, H.-J.; Henneberger, K. Bound Excitons in Local Density Approximation. *phys. stat. sol. (b)* **1979**, *91*, 331–337. https://doi.org/10.1002/pssb.2220910138.

(36) Bir, G. L.; Pikus, G. E. *Symmetry and Strain-Induced Effects in Semiconductors*; Wiley/Halsted Press: New York, 1974; Vol. 1.

(37) Pawlis, A.; Berstermann, T.; Brüggemann, C.; Bombeck, M.; Dunker, D.; Yakovlev, D. R.; Gippius, N. A.; Lischka, K.; Bayer, M. Exciton States in Shallow ZnSe/(Zn,Mg)Se Quantum Wells: Interaction of Confined and Continuum Electron and Hole States. *Phys Rev B* **2011**, *83*, 115302. https://doi.org/10.1103/PhysRevB.83.115302.

(38) Wörz, M.; Griebl, E.; Reisinger, T.; Flierl, R.; Haserer, B.; Semmler, T.; Frey, T.; Gebhardt, W. Gap Energies, Exciton Binding Energies and Band Offsets in Ternary ZnMgSe Compounds and ZnSe/ZnMgSe Heterostructures. *Phys. stat. sol. (b)* **1997**, *202*, 805–816. https://doi.org/10.1002/1521-3951(199708)202:2<805::AID-PSSB805>3.0.CO;2-O.

(39) Leavitt, R. P.; Little, J. Simple Method for Calculating Exciton Binding Energies in Quantum-Confined Semiconductor Structures. *Phys Rev B* **1990**, *42* (18), 11774–11783. https://doi.org/10.1103/PhysRevB.42.11774.

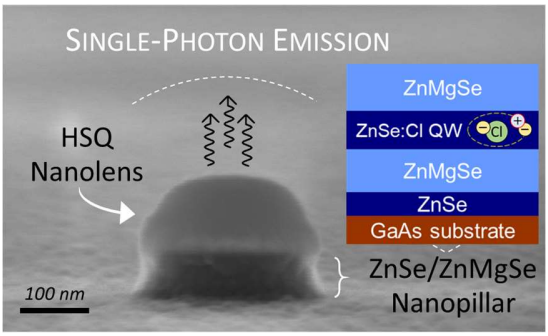
SINGLE-PHOTON EMISSION
HSQ
Nanolens
ZnMgSe
ZnSe:Cl QW
Cl
ZnMgSe
ZnSe
GaAs substrate
ZnSe/ZnMgSe
Nanopillar
100 nm

TOC image